Applied Thermal Engineering 162 (2019) 114304

Contents lists available at ScienceDirect

Applied Thermal Engineering

journal homepage: www.elsevier.com/locate/apthermeng

A numerical evaluation of next generation additive layer manufactured inter-layer channel heat exchanger

Evaldas Greiciunas[a,*], Duncan Borman[b,1], Jonathan Summers[c], Steve J. Smith[d]

[a] Centre for Doctoral Training in Fluid Dynamics, University of Leeds, Leeds, West Yorkshire LS2 9JT, United Kingdom
[b] School of Civil Engineering, University of Leeds, Leeds, West Yorkshire LS2 9JT, United Kingdom
[c] School of Mechanical Engineering, University of Leeds, Leeds, West Yorkshire LS2 9JT, United Kingdom
[d] BAE Systems, Warton Aerodrome, Warton, Preston PR4 1AX, United Kingdom

HIGHLIGHTS

- A concept heat exchanger design has been constructed using ALM.
- HE corrugation allows interconnection between alternate HE core layers.
- Proposed heat exchanger unit is numerically evaluated using detailed CFD.
- Detailed CFD is required to adequately capture the flow and heat transfer behaviour.

ARTICLE INFO

Keywords:
Additive Layer Manufacturing (ALM)
Heat exchangers
Forced convection
Computation Fluid Dynamics (CFD)
Numerical analysis
OpenFOAM

ABSTRACT

A Concept Heat Exchanger (HE) design manufactured using the Additive Layer Manufacturing (ALM) technique Selective Laser Melting (SLM) is proposed and numerically evaluated. It is composed of a HE corrugation which introduces inter-layer flow conduits between the parallel HE layers of the same fluid. These pathways are provided by hollow elliptical tubes which serve several functions: to disturb the flow to promote heat transfer, to provide additional heat transfer area and to minimise flow maldistribution inside the HE core. The corrugation is incorporated into a counter-flow prototype HE unit model meaning to exploit the installation volume and design freedom made possible via ALM. Three Computational Fluid Dynamics (CFD) models are utilised to evaluate the performance of the proposed HE unit. Firstly, a traditional two step HE design methodology is utilised which works by initially evaluating a fully symmetric channel of the proposed HE corrugation (termed single channel). Then the results this model are incorporated into a simplified HE unit model. The second approach evaluates the HE unit performance based on a fully detailed CFD analysis that fully resolves flow and heat transfer inside the HE core. The third modelling approach involves splitting the inter-layer HE unit model into parts, which results in HE header models and allows simplification of the HE core into a single corrugation period width HE core model (termed superchannel). The results of these models are then compared to a conventional pin–fin HE unit model, formed by blocking the elliptical inter-layer conduits. It was found that in all the HE unit models the pressure drop is similar whilst the heat transfer was enhanced by between 7% and 13% in terms of the overall ΔT by the inter-layer channels (increasing with the Reynolds number). All simulations were completed using a CFD package OpenFOAM.

1. Introduction

Heat Exchangers are critical components in various heat management systems and are used widely within a number of industries including aerospace, automotive, power generation and others. A HE works by transferring the energy between the multiple fluid streams with a sufficiently high thermal gradient between them and are normally separated by a solid material. Numerous HE types are utilised in industry such as shell and tube, tube-fin, platular, plate-fin. The heat transfer inside them is based on forced convection of the fluid streams which prevents the formation of the thick thermal gradients near the solid. This is achieved by heat transfer surfaces known as HE

* Corresponding author.
E-mail addresses: scegr@leeds.ac.uk (E. Greiciunas), d.j.borman@leeds.ac.uk (D. Borman).
[1] Principal corresponding author.

https://doi.org/10.1016/j.applthermaleng.2019.114304
Received 18 May 2019; Received in revised form 12 August 2019; Accepted 23 August 2019
Available online 26 August 2019

Nomenclature

ALM	Additive Layer Manufacturing
CFD	Computational Fluid Dynamics
HE	heat exchanger(s)
NTU	Number of Transfer Units
SLM	Selective Laser Melting
ϵ	effectiveness
d_h	hydraulic diameter
$\mathbf{u}$	velocity vector
ρ	density, kg/m^3
p	pressure, Pa
μ	viscosity, Pa·s
μ_t	turbulent viscosity, Pa·s
S	Source Term
T	temperature, K
d	Darcy factor
f	Forchheimer factor
Q_ϵ	heat source
c_p	specific heat capacity, J/(kgK)
$\epsilon(\dot{m}, \dot{m}_2)$	effectiveness table
$\dot{m}$	net mass flux entering heat exchanger, kg/s
$\dot{m}_2$	mass flow rate of the secondary stream, kg/s
T_1	primary inlet temperature, K
T_2	secondary inlet temperature, K
Re_{corrug}	Reynolds number defined as $Re_{corrug} = (\rho U d_h)/\mu$
Re_{inlet}	Reynolds number defined as $Re_{inlet} = (\rho U D_{inlet})/\mu$

corrugation which disturb the flow and enhance heat transfer performance. A common goal of HE design is to produce the most compact unit possible whilst maintaining the pressure drop to the minimum [1,2]. Compactness is one of the main criteria for the evaluation of a HE and measures the heat transfer area versus the flow volume and should be above $\approx$ 400 m^2/m^3 for liquids and $\approx$ 700 m^2/m^3 for gases [3]. An alternative is the hydraulic diameter of the HE corrugation which should be below $d_h = 8$ mm for liquids and $d_h = 5$ mm for gases [3]. Current HE compactness vary depending on the manufacturing method and some of the most common processes employed are welding and vacuum brazing of the individual HE components [2]. However, both methods have drawbacks: vacuum brazing is used for bonding the HE core which is typically assembled out of small individual components and whilst it can produce a compact HE it creates a risk of a leakage. Furthermore the brazing process occurs in a low pressure chamber which shrinks the HE core making the dimensional accuracy complicated. Welding is used in a variety of processes, both for HE core and HE headers. However, it induces high thermal stresses and needs to be carefully controlled in order to prevent leakage or manufacturing defects, a common issue in current HE [2,4]. In particular scenarios bolts can be used in gasketed designs for HE such as platular [5] or shell and tube [6]. This allows easy disassembly and clean up but also results in a larger required installation volume. In addition, current compact HE cores are typically limited to a rectangular cuboid shape (resulting from the manufacturing process). It creates installation problems and inefficiencies in many applications (such as aerospace where the available space is limited).

Compared to traditional manufacturing methods ALM has a number of advantages: it produces uniform parts, provides greater design freedom and reduces the required overall tooling, fixtures and energy cost [7]. The approach has gained much interest from researchers looking to understand and exploit different process for use in heat transfer related application areas. Interesting examples include use of SLM [8], Direct Metal Laser Sintering (DMLS) [9,10], Powder-Bed Fusion (PBF) [11]. The processes have been applied to a wide range of scenarios such as heat sinks [8], microchannel HE [9,10], direct replacement of an aircraft oil cooler [11]. However, the majority of studies take an incremental step in the HE design and do not fully utilise the freedom of ALM. One aspect of all the ALM techniques is a resulting coarse surface finish which can cause increased pressure drop [11], but this is typically offset by a notable increase in heat transfer density (in some cases as much as 30% [10]). SLM is an exciting approach due to its potential to create highly detailed structural components [7,12]. It is a powder based ALM process which works by selectively completely melting thin layers of metal powder in successive layers forming a part [13]. Furthermore, the process is capable of producing thin material layers (50 μm reported in [14]), enabling manufacture at HE relevant lengthscales.

The numerical HE design is typically undertaken using a two step approach: firstly a small section of a HE unit is modelled to obtain flow and heat transfer performance of the HE corrugation. Depending on the circumstances the corrugation model could contain a periodic section of the HE fins [15,16], have a finite length channel [17,18] or employ the conjugate heat transfer methodology such as [19]. The results of such a model are then applied to a macro-scale HE unit model where the flow and heat transfer inside the HE core are simplified using porous media and heat transfer effectiveness (described as a ratio of actual versus maximum possible heat transfer) models [20–22]. This two step approach is typically undertaken to reduce the computational size of the HE unit model due to the high amount of heat transfer elements present in the industrial HE.

In this paper an inter-layer HE corrugation design is presented and a feasibility study of its performance is carried out using SLM which led to the manufacturing of a proof of concept HE unit. Then the HE unit is numerically analysed using multiple solution strategies at the $25 \leqslant Re_{corrug} \leqslant 1000$. The concept HE unit is firstly evaluated using a traditional approach where a single channel corrugation model is used to obtain the characteristics which are then implemented into a simplified HE unit model. This is then compared to a fully resolved HE unit model, feasible computationally due to the relatively small size of the prototype HE. A reduction of computational cost is also proposed and evaluated by splitting the detailed inter-layer HE unit into sections (inlet and outlet HE headers and the superchannel models). The complex flow influence to the HE performance is then compared to a similar pin–fin HE unit, formed by blocking the complex flow channels.

2. The Concept HE design

The concept design work was motivated both by the potential new geometries enabled by ALM and inefficiencies in the current generation HE (Fig. 1a). The traditional manufacturing methods of the HE core (vacuum brazing) and the HE headers (welding) result in reduced efficiency of HE units in terms of the installation volume. A further motivation arises from looking inside a typical HE unit (Fig. 1b). The shape of the headers leads to maldistributed flow entering into the HE core which results in underutilised regions of the HE core. In order to reduce these effects a two step approach was undertaken and both HE corrugation and HE header concepts were proposed. One of the major advantages of ALM is that it allows flexible orientation of the flows. This enables designs similar to those of current cross-flow plate-fin HE compactness level surfaces to be rotated in a more efficient counter-flow orientation. This can be accomplished by introducing manifold HE headers which only become feasible through the ALM approach (currently the HE headers are typically welded onto the HE core). An example model of a header design is shown in Fig. 2a with the counter-flow orientation. The manifold design helps to avoid the over-expansion of the flow area and could lead to lower maldistribution levels. In addition, the counter-flow orientation decreases the packaging volume of

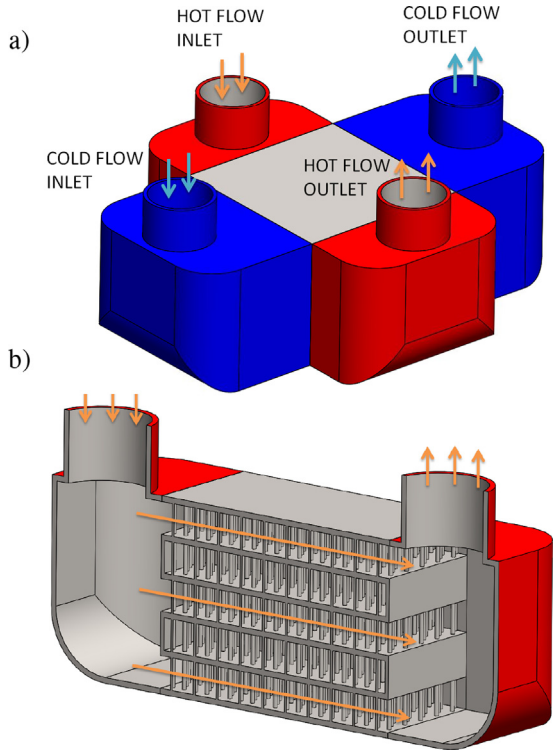

Fig. 1. a) Simplified layout of a typical cross-flow HE unit (plate-fin) with headers. b) Cut-through section of the hot flow pathway of a typical crossflow HE unit.

the HE unit. The manifold design principle could also be easily adapted for the cross-flow HE application as required.

The second aspect of the proposed design is the introduction of the inter-layer HE corrugation (CAD model in Fig. 2b with a 2D schematic of the corrugation in Fig. 2c). The design aims at reducing the maldistribution effects inside the HE core which are challenging to eliminate in a standard design, currently used in industry, such as plate-fin [23]. The proposed solution uses elliptical conduits tilted at 45deg (relative to the parallel HE core layers). This enables the flow to move between the parallel layers of the same fluid stream with the purpose of reducing the under-utilised HE core regions (To help understand the flow, refer Figs. 6, 9a which show temperature contours of the flow through the inter-layer corrugation models). It also helps to induce more complex mixing behaviour without the need for additional turbulators at the locations where the flow travelling through the vertical conduits meets the flow in the neighbouring layer (taking on the role of the fins). Compared to the traditional approach the inter-layer corrugation design eliminates secondary heat transfer surfaces (fins) as the solid material is always in thermal contact with both (hot and cold) fluids. This is a potential advantage over standard HE (such as plate-fin) where the majority of heat transfer surface area is exposed to one fluid stream only through fins. Such HE unit could easily be adapted for an application in the high-value sector such as aerospace or motorsport where low installation volume and thermal efficiency are critical. Additionally, using ALM has other advantages such as less complicated on-demand manufacturing capability in-house from basic metal powder which removes the need for complex and expensive logistics chain.

2.1. Inter-layer HE manufacture

The HE header and corrugation models were manufactured using commercially pure titanium at HE relevant lengthscales (Fig. 2d and 2e). Rough surface finishes can be observed in Fig. 2e which is an inherent feature of current SLM technology, formed by the melting of the powder grains. A post-processing procedure such as shot blasting can be used (HE header model in Fig. 2d) if a smoother surface finish is required. After ensuring feasibility of the HE corrugation and header concepts by manufacture, the proof of concept HE unit was developed (Fig. 3a), containing four cold and three hot fluid layers in counter flow orientation. The corrugation density was increased to $d_h = 2.8$ mm, obtained by averaging square (minimum area between the conduits $d_h = 2.93$ mm) and elliptical (based on characteristics of the conduits $d_h = 2.73$ mm) hydraulic diameters. This achieved a HE compactness

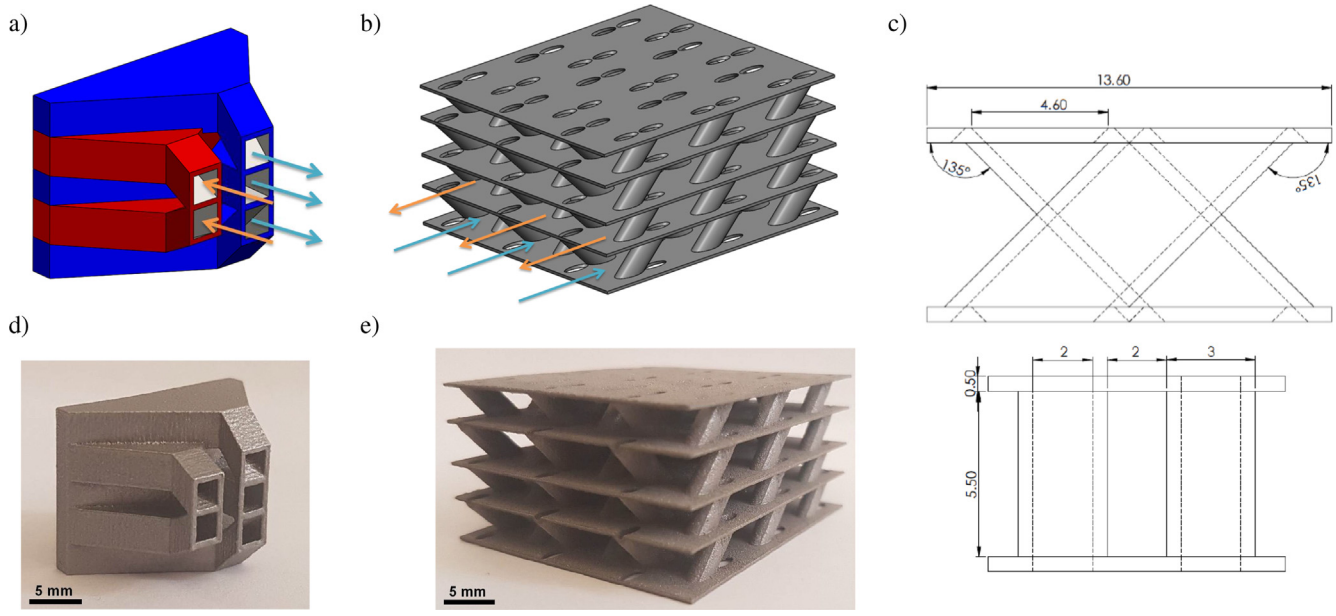

Fig. 2. a) Model of the manifold header - red and blue colours indicate the hot and cold pathways respectively. b) Model of the inter-layer channel corrugation section in counter-flow orientation. c) Schematic of the periodic inter-layer HE corrugation in side (top) and front (bottom views) with dimensions given in millimetres. d) Manufactured model of the manifold design with channel height of 2.5 mm and wall thickness of 0.5 mm. e) Manufactured HE section with a hydraulic diameter $d_h = 5$ mm and 0.5 mm uniform wall thickness. (For interpretation of the references to colour in this figure legend, the reader is referred to the web version of this article.)

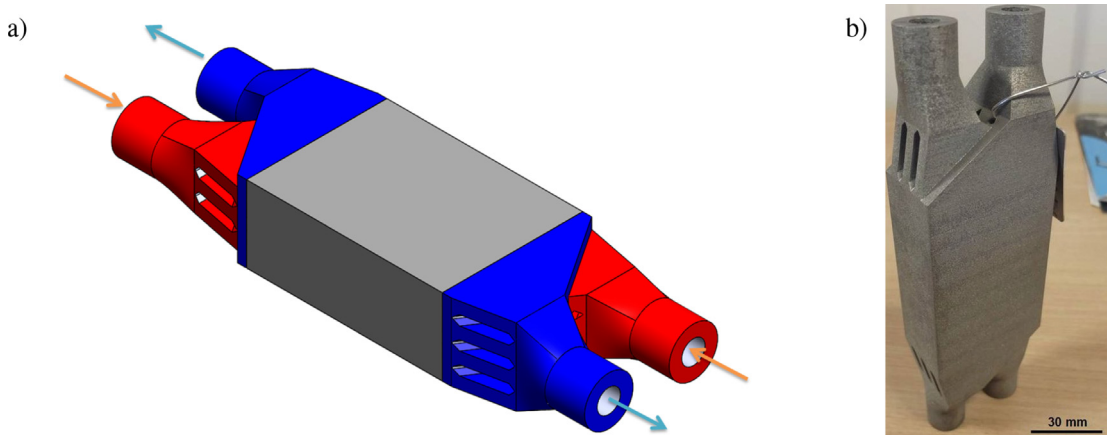

Fig. 3. a) Proof of concept inter-layer HE unit CAD model in counter-flow orientation (262 × 42.5 × 78 mm). b) Manufactured inter-layer HE unit in printing orientation.

(β) value, defined as:

$$\beta = \frac{A_h}{V} = \frac{\text{heat transfer area}}{\text{volume for the flow}} = 818\frac{\text{m}^2}{\text{m}^3} \quad (1)$$

enabling the concept HE to be classed as compact for both liquids and gases [3]. The header design was adjusted for fitting with either 3/8 or 1/2 BSP connectors. In addition, the header manifolds were adapted to eliminate the ALM support material, thus the HE unit could be built vertically upwards starting from one side of the HE header ports. The inter-layer HE unit was manufactured and is shown in the printing orientation in Fig. 3b. No defects were observed, confirming manufacturing feasibility of a proof of concept HE unit.

3. Numerical solution methodology

The approach to the numerical analysis follows the methodology set out in [23] where the authors have validated the modelling approach against an experimental HE unit. Numerical simulations of the proof of concept HE were completed using the CFD platform OpenFOAM with the following equations utilised [24]:

$$\nabla \cdot \mathbf{u} = 0 \quad (2)$$

$$\rho\frac{\partial \mathbf{u}}{\partial t} + \rho(\mathbf{u}\cdot\nabla)\mathbf{u} = -\nabla p + \mu_{eff}\nabla^2\mathbf{u} + \mathbf{S} \quad (3)$$

$$\frac{\partial T}{\partial t} + \mathbf{u}\cdot\nabla T = \alpha_{eff}\nabla^2 T + Q_\epsilon \quad (4)$$

where $\mathbf{u}$ - velocity vector, p - pressure, T - temperature, ρ - constant density. $\mu_{eff} = \mu + \mu_t$, where μ_t is the dynamic turbulent viscosity and calculated based on the $k-\omega$ SST turbulence model [25] and $\alpha_{eff} = \alpha + \mu_t/(\rho Pr_t)$, where $\alpha = k/(\rho c_p)$ and Pr_t is the turbulent Prandtl number taken to be 0.85 in RANS simulations. It should also be noted that walls of all the computational domains were modelled smooth. A traditional HE modelling cycle simplifies flow and heat transfer inside the HE core by using source terms for both flow and energy. The flow inside the HE core was simplified using the Darcy-Forschheimer model:

$$\mathbf{S} = -(\mu d + \frac{1}{2}f\rho|\mathbf{u}|)\mathbf{u} = \nabla p \quad (5)$$

where $d = 0$ was set to comply with standard HE models [26] whilst f is calculated from the HE corrugation analysis. Heat transfer inside the HE core is simplified using the effectiveness source term:

$$Q_\epsilon = \dot{m}c_p\,\epsilon(\dot{m}, \dot{m}_2)(T_2 - T_1) \quad (6)$$

where the T_1 & T_2 are the primary and secondary fluid inlet temperatures, $\dot{m}$ & $\dot{m}_2$ are the primary and secondary fluid mass flows and $\epsilon(\dot{m}, \dot{m}_2)$ is the effectiveness look up table. This table uses adata from a HE corrugation model, such as single channel domain as shown in Figs. 4a & 6 which are described later in Section 3.1. All simulations were completed using water as a working fluid with the constant

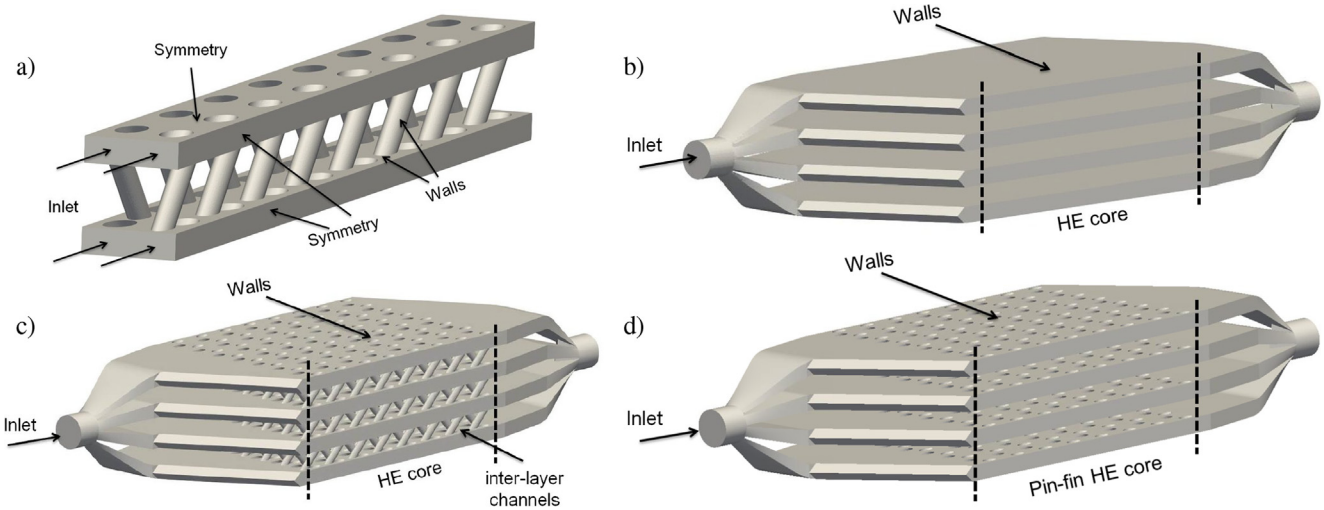

Fig. 4. Computational domains of: a) Fully symmetric full length single channel corrugation domain. b) Simplified HE unit model. c) Fully resolved cold side of the complex inter-layer HE. d) Fully resolved cold side of the conventional pin–fin HE model.

properties in Table 1. The main simplification employed throughout this study is the assumption of the constant temperature flow through the hot HE side. This allows elimination of two out of three computational domains: hot flow and solid. This significantly reduces the computational cost by reducing the mesh size approximately twice whilst still enabling the evaluation of the inter-layer HE configuration performance. Throughout all of the computational domains temperature at the flow inlet was set $T_{inlet} = 293$ K. A constant wall temperature condition was used to provide a thermal gradient and was set to $T_{wall} = 318$ K. The heat transfer assumption reduces the heat transfer effectiveness relation to:

$$\epsilon = \frac{\text{actual heat transfer}}{\text{maximum possible heat transfer}} = \frac{T_{outlet} - T_{inlet}}{T_{wall} - T_{inlet}} \quad (7)$$

Meshing of the computational domains was completed using the OpenFOAM tools `blockmesh` and `snappyHexMesh` to produce hexahedral dominant computational domains. The simulations were initialised using the potential flow solver (`potentialFoam`) that provides a good initial estimate. The final solutions of the simulations were obtained using the discretised domain given in Table 2.

3.1. Computational domains and grid independence

Firstly, the single channel corrugation model (Fig. 4a) is discussed. In this model a fully symmetric channel of the inter-layer HE core is modelled. It is completed by modelling half of the two cold flow HE core layers which are connected by the vertical conduits. The visualisation of the output is given in Fig. 6 and shows the inter-layer heat transfer occurring even in the case where there is no maldistribution at the inlet. Mesh independence of the HE corrugation model was completed at $Re_{corrug} = 200$ ($Re_{corrug} = \rho U d_h/\mu$, where d_h - hydraulic diameter of the flow) using the laminar flow model with the series of generated meshes presented in Table 3. Both medium and the fine meshes predicted very similar responses in terms of both ΔP and ΔT. However, fine resolution was used for the further simulations as the model was planned to be applied to higher Reynolds number cases as well.

The second model implemented was the simplified porous media HE unit model (Fig. 4b). In this model the complex geometry is reduced to four flat layers where the detailed flow and heat transfer inside the HE core are modelled using the source terms described previously. For the purposes of mesh independence an arbitrary uniform resistance and heat transfer were set across the HE core. The flow was simplified with the Darcy-Forschheimer model (Eq. 5, with coefficients of $d = 0$ and $f = 236$) along with a uniform $\Delta T = 10$ K prescribed using the effectiveness model (Eqs. 6 and 7). The $Re_{inlet} = 7532$ ($Re_{inlet} = \rho U_{inlet} D_{inlet}/\mu$ and equivalent to $Re_{corrug} \approx 150$, assuming uniform expansion in the HE inlet header) was simulated at a range of mesh resolutions shown in Table 4. Medium mesh resolution was selected as it showed stabilisation in terms of the overall pressure drop and temperature change.

The third model considered a fully detailed flow and heat transfer at the HE unit level (termed inter-layer HE) and required a substantial computational resource. The extracted cold flow HE unit domain is shown in the Fig. 4c. In this model the same thermal boundaries were applied with a constant wall temperature boundary ($T_{wall} = 318$ K) is applied to the inner HE core walls whilst the remaining domain walls were set to an adiabatic condition. The fully detailed inter-layer HE model is particularly valuable as it provides information about the performance of the inter-layer HE corrugation as a part of the HE unit and serves as a benchmark against more simplified models. A series of meshes were generated and listed in Table 5 to evaluate the performance at $Re_{inlet} = 7532$ ($Re_{corrug} \approx 150$). The medium resolution mesh was selected for further simulations as both the pressure drop and temperature change were in close agreement compared to the fine mesh.

To provide a comparison of the inter-layer HE a simplified pin–fin HE unit model was created (Fig. 4d). This model is very similar to the detailed model of the inter-layer HE, however, in this design the conduits were blocked forming solid pins which eliminate the inter-layer mixing. Using the same meshing procedure and refinement levels as for the medium inter-layer HE unit mesh yielded mesh-independent results. This enables direct evaluation of the complex flow effects by comparison with the inter-layer HE unit model.

A final approach to assist in evaluation of the inter-layer HE performance involved splitting the detailed inter-layer HE unit model (Fig. 4c) into three parts: inlet and outlet HE headers and the HE core. In this approach only a single corrugation width of HE core is evaluated (Fig. 5a). The model is named as the 'superchannel' in the paper and significantly reduces the computational cost. It is useful in providing idealised HE core performance as it uses a uniform velocity inlet into the HE core. It allows the separate evaluation of the ΔP contributions by the HE headers. The simulations using these domains were undertaken using identical mesh settings to the medium resolution of the inter-layer HE unit model making the results directly comparable. This allowed for a significant reduction in the size of the meshes: 4.2×10^6 and 4.9×10^6 element meshes for the superchannel and header models respectively versus the 27.7×10^6 for the full inter-layer HE unit model.

4. Results

4.1. Single channel model predictions

The results of the fully symmetric single channel model (Fig. 4a) are given in the Figs. 7a & 7c where the non dimensional effectiveness (Eq. 7) and and the friction factor f, derived from Eq. 5:

$$f = \frac{2|\nabla p_{flow-wise}|}{\rho |\mathbf{u}|^2}. \quad (8)$$

Steady-state and transient flow assumptions were evaluated with the results of the former shown first. The simulations were completed using both laminar and $k-\omega$ *SST* flow modelling assumptions over a $25 \leqslant Re_{corrug} \leqslant 1000$ Reynolds number range. At the lower Reynolds numbers, both laminar and $k-\omega$ *SST* models produced close to identical results. However, at the $Re_{corug} > 500$, the laminar model diverged (Fig. 7a). Even at $Re_{corrug} = 500$ a discrepancy in terms of the thermal predictions is seen between the laminar and $k-\omega$ *SST* models (Fig. 7c). Here the laminar model predicted a sudden drop in the effectiveness and did not follow the general solution trends. This is thought to relate to the end of the laminar flow regime. It coincides with the results of the previous work by the authors [27] where the transitional flow was shown to occur at the Reynolds numbers in the order of several hundred. Interestingly despite this identification the $k-\omega$ *SST* steady-state predictions converged to $Re_{corrug} = 1000$.

4.1.1. Transitional flow effects

As unsteady flow behaviour was anticipated, fully transient solutions of the single channel domain were also completed. Again, laminar and $k-\omega$ *SST* models at $200 \leqslant Re_{corrug} \leq 1000$ were undertaken. Variable time-step control of the simulations was employed by restricting the maximum Courant number [28] to 0.5 (based on the findings in [27]). In these simulations the medium single channel resolution mesh was used 2.1×10^6 (Table 3) to make the simulations

Table 1
Properties of water used for the predictions.

		Units
ρ	994	kg/m^3
μ	0.719×10^{-3}	Pa·s
c_p	4178	J/(kgK)
Pr	4.885	–

Table 2
Discretisation schemes used for the simulations.

	Discretisation scheme
Gradient	Gauss linear
Pressure	Gauss linear corrected
Momentum	Gauss linearUpwind
Energy	Gauss linearUpwind
Turbulent kinetic energy	bounded Gauss upwind
Specific dissipation rate	bounded Gauss upwind
Transient	Euler

Table 3
Mesh resolution data of the ALM HE corrugation showing the overall flow resistance and heat transfer performance of the single channel model.

Mesh	Mesh size	ΔP, Pa	ΔT, K
Coarse	43951	20.3	16.3
Coarse2	296930	25.8	18.5
Medium	2.1×10^6	26.4	18.8
Fine	13.4×10^6	26.2	18.6
Fine2	20.4×10^6	26.1	18.6

Table 4
Overall characteristics of the simplified HE unit model employing the porous media and effectiveness assumptions.

Mesh	Mesh size	ΔP, Pa	ΔT, K
Coarse	1.7×10^6	148.9	9.9
Coarse2	6.7×10^6	156.8	10.2
Medium	27.7×10^6	167.2	9.8
Fine	44.6×10^6	170.6	9.9

Table 5
Mesh independence study data of the ALM HE unit model showingmesh the overall performance.

Mesh	Mesh size	ΔP, Pa	ΔT, K
Coarse	1.7×10^6	143.7	15.1
Coarse2	8.8×10^6	143.8	16.1
Medium	27.4×10^6	157.9	16.5
Fine	69.6×10^6	163.4	17.4

computationally feasible. They were run to a residence time $T_{res} = 1.5$ (defined as T_{res} = (lenght of the domain)/(velocity at the inlet), $[s]$) to evaluate whether the unsteady flow effects are important.

Contrasting to the steady-state results the transient simulations converged for the full Reynolds number range using both laminar and

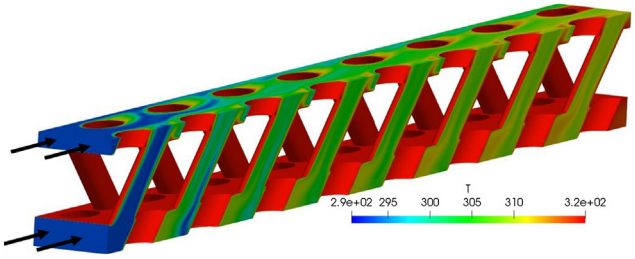

Fig. 6. Cut-through section of the single channel model showing domain heating up at $Re_{corrug} = 200$ (fine mesh resolution).

$k - \omega$ *SST* modelling assumptions. A clear onset of the transient flow was found at $Re_{corrug} \geqslant 500$ (as suspected from the previous section) whilst small fluctuations in the predictions were observed at $Re_{corrug} = 400$. However, as shown in the Figs. 7b & 7d ($Re_{corrug} = 1000$), no significant differences are observed between the two flow models. The pressure drop is predicted (Fig. 7b) b) to be oscillatory whilst an almost steady state temperature difference (Fig. 7d) prediction is produced towards the end of the simulation time. The laminar model predicts a slightly higher pressure drop than the $k - \omega$ *SST*, similar to observed in previous findings [27]. The time-averaged results of both pressure drop and the final result of heat transfer are almost identical to the $k - \omega$ *SST* steady-state at $Re_{corrug} = 1000$ ($\Delta P = 357$ *Pa*, $\Delta T = 11.6$ K), verifying that the steady-state HE corrugation predictions are appropriate for the later studies.

4.2. Comparing the different HE unit models

Results of the HE unit models are analysed at $1738 \leqslant Re_{inlet} \leq 27577$ (equivalent to $25 \leqslant Re_{corrug} \leq 500$ assuming no maldistribution in the HE inlet header). The data provided in this section was sampled and averaged across all the flow layers at each location shown in Fig. 5b for all the HE unit models. The results of the three HE unit models can be found in Figs. 8a & 8b with the temperature contours in Figs. 8d - 8f. Minimal difference is observed between the inter-layer and pin–fin HE models in terms of the overall pressure drop (Fig. 8a). However, a more notable difference is seen when comparing the two detailed HE unit models to the simplified HE. Higher overall pressure drop is predicted, originating inside the HE core and is a result of the simplification of the HE core model into four porous flow layers.

In terms of the thermal performance, the inter-layer HE unit is observed to heat-up slightly faster and leads to more heat being transferred at the end of the domain compared to the pin–fin HE. This appears to be driven by higher heat entrainment in the inlet HE header by the inter-layer HE model as seen in Fig. 8b. This results in a significantly different overall ΔT between the two models presented in Fig. 10b. It is further observed that the inter-layer and the pin–fin HE unit domains

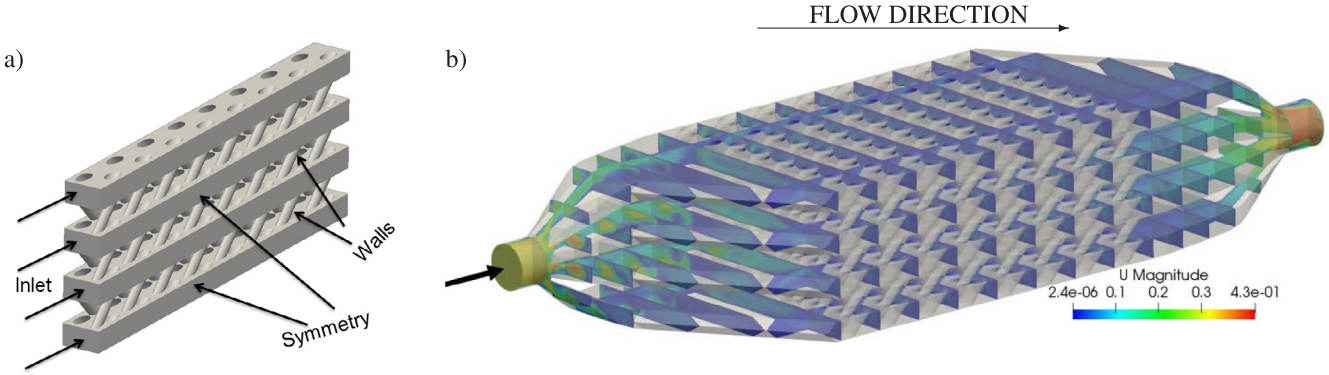

Fig. 5. a) Superchannel HE Core model, consisting of single inter-layer HE core width period section. b) Extraction planes used to study the flow-wise development of pressure drop and heat transfer of the HE unit models (Figs. 4b - 4d) with velocity magnitude outputs provided at $Re_corrug = 100$).

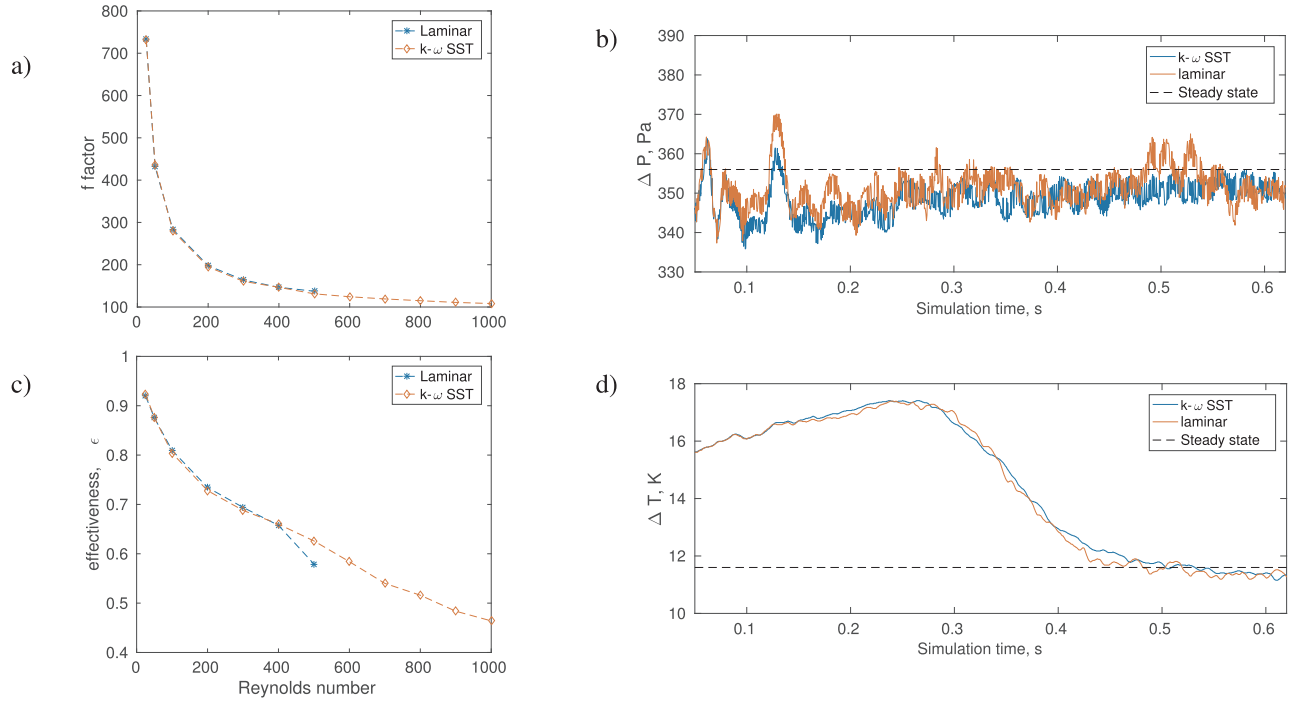

Fig. 7. Single channel model results across the Reynolds number range of a) steady state friction factor of b) transient solution pressure drop data at Re_{corrug} = 1000 c) effectiveness factors using two modelling assumptions and d) transient solution temperature change data at Re_{corrug} = 1000.

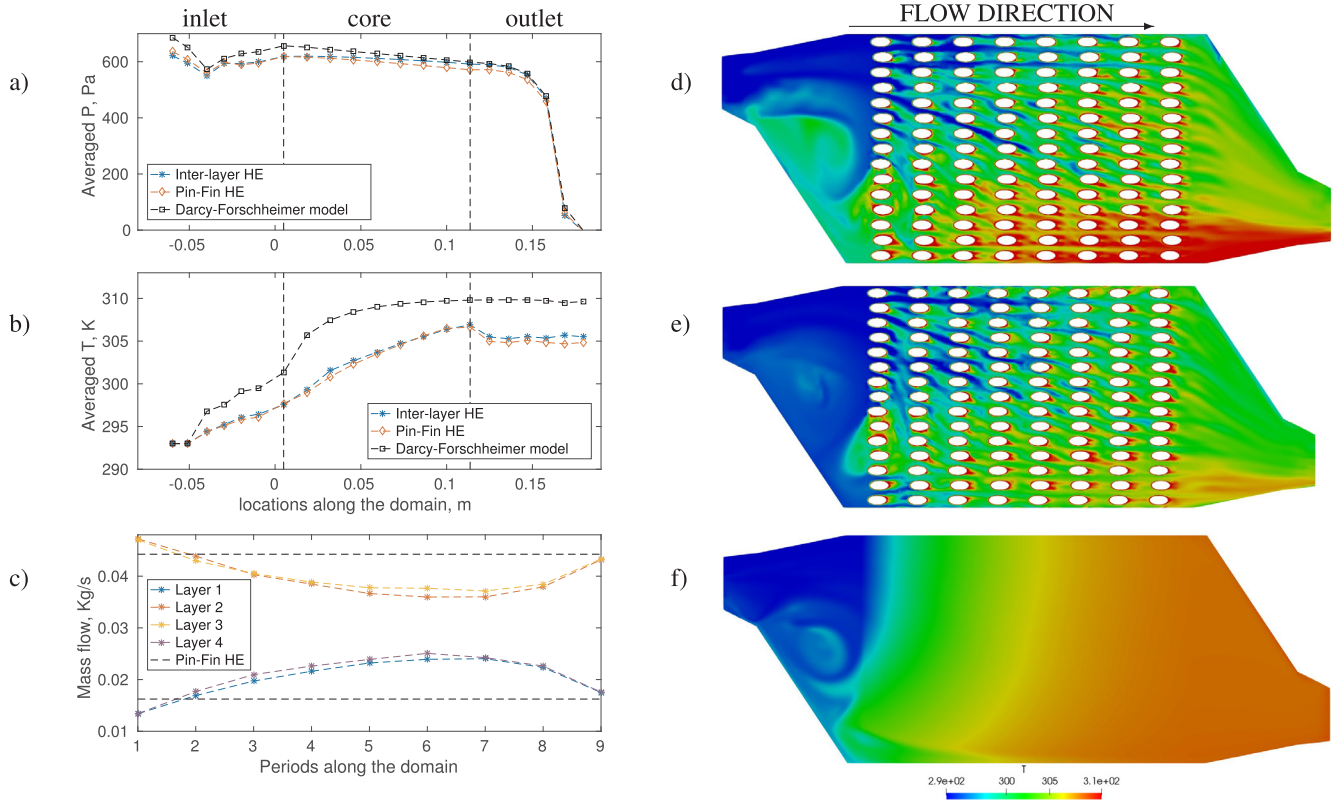

Fig. 8. a) Mean Pressure and b) Temperature extracted at the stream-wise locations in Fig. 5 porous of the HE models. First third of the sampling locations is the inlet header, middle - HE core, and last third is the outlet HE header. c) Mass flow throughout the inter-layer HE in the centre HE core layers (Layers 2 & 3) versus the outer HE layers (Layers 1&4) (Dotted lines show the mass flow through the pin–fin HE unit). Cut through section contours through the second layer of the HE core models (Fig. 4) showing temperature using: d) Inter-layer e) Pin–fin HE and f) Simplified models (Flow direction is from the left to the right). All simulations were completed at Re_{corrug} = 300, Re_{inlet} = 16546.

heat up to a much lower outlet HE temperature when compared to the simplified HE (the simplified model over predicts the heat transfer). This can be explained by the higher heat entrainment through the inlet HE header which leads to larger heating prior the HE core. A further reason is likely to be the simplification of the HE core into four layers. This results in a fixed ΔT across each HE layer which does not occur in the detailed HE models (see Figs. 8d - 8f). Theoretically, each HE layer could be broken down into more porous zones, however this would be a complex and time consuming task.

4.2.1. Flow redistribution inside the inter-layer HE core

The effect of the inter-layer channels on reducing the maldistribution inside the HE core is investigated by sampling the mass-flow at every corrugation period inside the inter-layer HE core separately for all four cold flow layers (numbered 1 to 4 from the bottom to the top of the HE core and shown in Fig. 5). The behaviour was found to be independent of the Reynolds number and an example is shown in Fig. 8c. It can be clearly seen that whilst the flow at the inlet to the HE core (period 1) is highly maldistributed, the inter-layer channels promote flow to enter the outer HE layers. The redistribution reaches the peak at around periods 6–7 of the HE core corrugation. After this point the trend reverses and the mass flow returns to the middle layers. This is because the flow exit is less constricted through the outlet HE header middle layers. In contrast, the pin–fin maldistribution levels of the outer and inner layers of the HE for the same flow rate are given as dotted lines in Fig. 8c. They show there is an imbalance in the HE core without the inter-layer channels (typical behaviour on traditional HE). The next step undertaken is to calculate the maximum mass-flow entrainment levels into the outer layers by using the following:

$$\dot{m}_{ratio} = \frac{\max(\dot{m}_{\text{inner layers}})}{\min(\dot{m}_{\text{outer layers}})}. \tag{9}$$

The summary of the results are given for the inter-layer HE in Table 6. At the lowest Reynolds numbers the mass flow redistribution was the highest (as expected) with the entrainment ratio stabilising to $0.67 - 0.68$ at the higher end of the Reynolds number range. This can be compared to the same measure calculated for the pin–fin HE which throughout the Reynolds number range tested was constant at 0.38, meaning that at its peak the malstristribution inside the inter-layer HE was half that of the pin–fin HE.

4.2.2. Superchannel model results

Observing that the full detailed simulations of the inter-layer HE are computationally expensive, an alternative formulation of the computational domain was developed. In the section the single corrugation width HE core model (termed superchannel) and the outlet header are analysed. The inlet header in this case was omitted as its contribution to the overall pressure drop of the system was small. When designing a new unit it can be beneficial to analyse the inlet header to establish the flow maldistribution levels at the HE core inlet, but for this study this was not undertaken. The superchannel model is an idealised HE core model shown in Fig. 9a where no initial flow maldistribution occurs. It is clear that inter-layer mixing can be observed in results, even in the case of the uniform velocity inlet case which reinforces the potential benefit of the inter-layer HE corrugation. The outlet HE header is modelled by using a uniform velocity inlet condition entering the header (without the heat transfer considered). It was undertaken as the pressure drop in all the HE unit models was dominated by the exit header pressure drop. The same high pressure drop can be observed visually in Fig. 9b when running the outlet HE header separately. However, in this case, due to the uniform velocity inlet condition, more flow is inevitably directed through the outer HE header layers. This has the potential to result in a higher pressure drop and is analysed further in the following section.

4.3. Overall performance comparison of the different HE models

Results of the overall pressure drop and heat transfer are contrasted at $25 \leqslant Re_{corrug} \leqslant 500$ between the different HE models in Fig. 10. It should be noted that pressure drop through the HE core is not compared in this section as it was shown to be small compared to the outlet HE header effects, seen in Fig. 8a. Comparing the HE unit pressure drop data highlights that the overall differences in terms of the pressure drop between the inter-layer and pin–fin HE units are negligible across the Reynolds number range (Fig. 10a).

The simplified HE unit model predicts increasingly higher pressure drop, however, the difference from the other HE unit models is relatively small (less than 10%) yielding acceptable results. The outlet HE header model predicted the highest pressure drop among all the comparable models (up to 30%) which increases with the Reynolds number. This is likely to be caused by an inlet boundary condition to the HE outlet headers, discussed in the previous section. However, the data obtained is still useful and can be used for a more conservative pressure drop prediction during the design cycle.

Overall thermal performance for all the numerical models is compared using ΔT in Fig. 10b. The results can be divided into two groups: single channel, superchannel domains and the inter-layer, pin–fin and simplified HE unit models. The first group are the corrugation only domains and the single channel domain is the most idealised and has the highest computational grid resolution. This model also produces the highest temperature change compared to the others, whereas the superchannel model produces increasingly lower ΔT with increasing Reynolds number compared to the single channel model. The increasing difference arises from the finite height of the superchannel model which limits the flow inter-layer mixing in the outer HE core layers. It also requires an adiabatic boundary at the top and bottom of the superchannel model to simulate the idealised HE core accurately limiting the proportion of the wall area utilised for heat transfer.

The next group are the inter-layer, pin–fin and simplified HE unit models. Between the inter-layer and pin–fin HE units, constantly higher overall temperature change across the HE is predicted by the inter-layer HE model (7–13% in terms of the overall ΔT, increasing with the Reynolds number). This shows added efficiency obtained through the inter-layer mixing, particularly in the cases of highly maldistributed flow and an increased heat transfer area. However, it should be noted that the superchannel model predicts a larger ΔT (2–13%) when compared to the inter-layer HE model. This suggests that further heat transfer enhancement could be obtained through improved inlet HE header design. The simplified porous media HE unit model does not follow the trends of the other two HE models. It increasingly over-predicts the temperature change, caused by the over-entrainment of heat into the inlet header and simplified HE core. This shows limitations of the current HE CFD methodology for complex ALM designs.

Table 6
Maximum entrainment of mass flow into the outer layers compared to the mass flow in the inner layers at the same HE core period. Constant value for pin–fin unit found was 0.38.

Re_{corrug}	$\dot{m}_{ratio}$
25	0.75
50	0.72
100	0.69
200	0.67
300	0.67
400	0.67
500	0.68

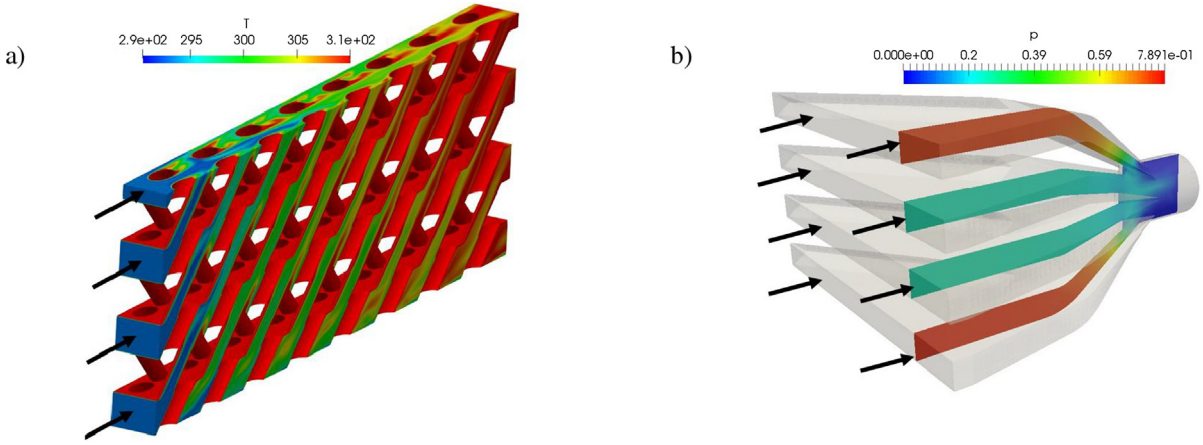

Fig. 9. Extracted flow domains ar Re_{corrug} = 200 of: a) Cut-through the superchannel model (Fig. 5a) showing the temperature change and the interlayer mixing b) outlet inter layer HE unit header (Fig. 4c) with a sampling plane showing high pressure (p/ρ) gradient at the exit of the domain. Flow direction i.s left to right.

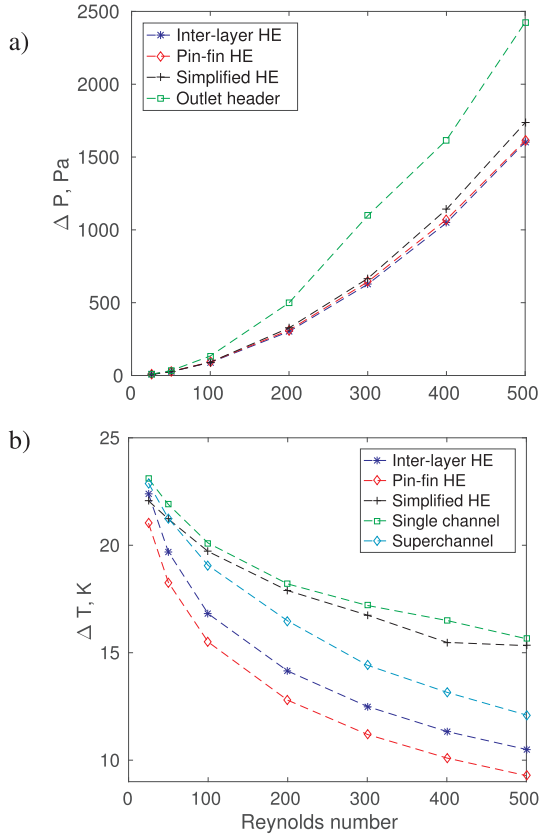

Fig. 10. a) Pressure drop ΔP data of the different HE unit models tested throughout the study. b) Temperature change across all (HE unit and HE corrugation) numerical models tested. Reynolds number was calculated according to the hydraulic diameter at the HE core (Re_{corrug}, assuming even expansion in the inlet HE header).

5. Conclusions

Inter-layer HE design has been proposed as a concept that aims to reduce the inherent inefficiencies associated with current HE arrangements, such as plate-fin. It utilises SLM technology which allows a greater design freedom and manufacturing control than the current HE manufacturing processes. Suitability of a traditional HE CFD methodology for complex ALM HE designs is evaluated, accomplished by comparing it to fully detailed HE unit CFD analysis. In addition, a superchannel HE unit modelling approach was developed which uses a slice of the HE core and produces an idealised HE core performance prediction. These models are then compared to a conventional pin–fin HE unit model, obtained by blocking the inter-layer HE conduits. The main findings of the study are:

- A structurally integral proof of concept inter-layer HE unit has been produced demonstrating viability of the concept design. It has a HE core hydraulic diameter d_h = 2.8 mm and can be classed as compact for both liquid and gases. The HE was built in a single manufacturing process which contrasts with traditional fabrication approaches that involve multiple labour intensive steps.
- The inter-layer HE outperformed the pin–fin HE layout by 7–13% in terms of the overall ΔT. The improved heat transfer was due to the design enabling mass flow redistribution within the HE core with no penalty on the pressure drop. This confirms the potential for the new design to have improved performance in comparison to conventional HE. It should be noted that the new design is a proof of concept HE and not a fully optimised design.
- The simplified traditional HE unit model produced similar pressure drop performance when compared to the inter-layer HE unit. However, it over-predicted the temperature change ΔT, caused by excessive heat entrainment in the inlet HE headers and over-simplification of the HE core. This limits the use of the traditional simplified modelling approach for the HE core flow and heat transfer for complex HE applications.
- Splitting the HE computational domain into the superchannel and outlet HE header models was undertaken to reduce the computational cost to evaluate complex HE flows. Although using the superchannel approach showed over predictions (2–13% in terms of ΔT) compared with the inter-layer HE unit model, combined with the outlet HE header model the methodology provides useful thermal and flow resistance estimates during the HE design process.

Acknowledgements

The authors would like to thank the primary sponsor BAE Systems for their support. This work also was supported by the Engineering and Physical Sciences Research Council (EPSRC) Centre for Doctoral Training in Fluid Dynamics at the University of Leeds under Grant No. EP/L01615X/1.

Appendix A. Supplementary material

Supplementary data associated with this article can be found, in the online version, at https://doi.org/10.1016/j.applthermaleng.2019.114304.

References

[1] W.M. Rohsenow, J.P. Hartnett, Y.I. Cho, et al., Handbook of Heat Transfer vol. 3, McGraw-Hill, New York, 1998.
[2] J.E. Hesselgreaves, Compact Heat Exchangers: Selection, Design and Operation, Gulf Professional Publishing, 2001.
[3] R.K. Shah, Compact Heat Exchanger Surface Selection, Optimization, and Computer Aided Thermal Design, Hemishpere, New York, 1983.
[4] R.K. Shah, D.P. Sekulic, Fundamentals of Heat Exchanger Design, John Wiley & Sons, 2003.
[5] H. Najafi, B. Najafi, Multi-objective optimization of a plate and frame heat exchanger via genetic algorithm, Heat Mass Transf. 46 (6) (2010) 639–647.
[6] J.H. Lienhard IV, J.H. Lienhard V, A Heat Transfer Textbook, Courier Corporation, 2015.
[7] T. Srivatsan, T. Sudarshan, Additive Manufacturing: Innovations, Advances, and Applications, CRC Press, 2015.
[8] M. Wong, I. Owen, C. Sutcliffe, A. Puri, Convective heat transfer and pressure losses across novel heat sinks fabricated by selective laser melting, Int. J. Heat Mass Transf. 52 (1–2) (2009) 281–288.
[9] X. Zhang, R. Tiwari, A.H. Shooshtari, M.M. Ohadi, An additively manufactured metallic manifold-microchannel heat exchanger for high temperature applications, Appl. Therm. Eng. 143 (2018) 899–908.
[10] M.A. Arie, A.H. Shooshtari, M.M. Ohadi, Experimental characterization of an additively manufactured heat exchanger for dry cooling of power plants, Appl. Therm. Eng. 129 (2018) 187–198.
[11] D. Saltzman, M. Bichnevicius, S. Lynch, T.W. Simpson, E.W. Reutzel, C. Dickman, R. Martukanitz, Design and evaluation of an additively manufactured aircraft heat exchanger, Appl. Therm. Eng. 138 (2018) 254–263.
[12] Y. Zhai, D.A. Lados, J.L. LaGoy, Additive manufacturing: making imagination the major limitation, Jom 66 (5) (2014) 808–816.
[13] I. Gibson, D.W. Rosen, B. Stucker, Additive Manufacturing Technologies, Springer, 2010.
[14] I. Yadroitsev, P. Bertrand, I. Smurov, Parametric analysis of the selective laser melting process, Appl. Surface Sci. 253 (19) (2007) 8064–8069.
[15] S. Patankar, C. Liu, E. Sparrow, Fully developed flow and heat transfer in ducts having streamwise-periodic variations of cross-sectional area, J. Heat Transfer 99 (2) (1977) 180–186.
[16] J. Zhang, J. Kundu, R.M. Manglik, Effect of fin waviness and spacing on the lateral vortex structure and laminar heat transfer in wavy-plate-fin cores, Int. J. Heat Mass Transf. 47 (8) (2004) 1719–1730.
[17] Z. Zheng, D.F. Fletcher, B.S. Haynes, Transient laminar heat transfer simulations in periodic zigzag channels, Int. J. Heat Mass Transf. 71 (2014) 758–768.
[18] Z. Dai, D.F. Fletcher, B.S. Haynes, Impact of tortuous geometry on laminar flow heat transfer in microchannels, Int. J. Heat Mass Transf. 83 (2015) 382–398.
[19] M. Ferrero, A. Scattina, E. Chiavazzo, F. Carena, D. Perocchio, M. Roberti, G.T. Rivalta, P. Asinari, Louver finned heat exchangers for automotive sector: Numerical simulations of heat transfer and flow resistance coping with industrial constraints, J. Heat Transfer 135 (12) (2013) 121801.
[20] L.S. Ismail, C. Ranganayakulu, R.K. Shah, Numerical study of flow patterns of compact plate-fin heat exchangers and generation of design data for offset and wavy fins, Int. J. Heat Mass Transf. 52 (17) (2009) 3972–3983.
[21] E. Carluccio, G. Starace, A. Ficarella, D. Laforgia, Numerical analysis of a cross-flow compact heat exchanger for vehicle applications, Appl. Therm. Eng. 25 (13) (2005) 1995–2013.
[22] A.M. Hayes, J.A. Khan, A.H. Shaaban, I.G. Spearing, The thermal modeling of a matrix heat exchanger using a porous medium and the thermal non-equilibrium model, Int. J. Therm. Sci. 47 (10) (2008) 1306–1315.
[23] E. Greiciunas, D. Borman, J. Summers, S.J. Smith, A multi-scale conjugate heat transfer modelling approach for corrugated heat exchangers, Int. J. Heat Mass Transf. 139 (2019) 928–937.
[24] S. Chandrasekhar, Hydrodynamic and Hydromagnetic Stability, Courier Corporation, 2013.
[25] F.R. Menter, Two-equation eddy-viscosity turbulence models for engineering applications, AIAA J. 32 (8) (1994) 1598–1605.
[26] ANSYS Inc., ANSYS Fluent Theory Guide, Guide, Ansys Inc., 2013.
[27] E. Greiciunas, D. Borman, J. Summers, Unsteady flow modelling in plate-fin heat exchanger channels, ASME 2017 Summer Heat Transfer Conference, American Society of Mechanical Engineers, 2017.
[28] R. Courant, K. Friedrichs, H. Lewy, Über die partiellen differenzengleichungen der mathematischen physik, Math. Ann. 100 (1) (1928) 32–74.